ACS APPLIED ELECTRONIC MATERIALS

pubs.acs.org/acsaelm Article

All-Solid-State Asymmetric Supercapacitors with Novel Ionic Liquid Gel Electrolytes

Yongrui Yang,[§] Tao Zhu,[§] Cheng Chi,[§] Lei Liu, Jie Zheng, and Xiong Gong*

Cite This: https://dx.doi.org/10.1021/acsaelm.0c00759 Read Online

ACCESS | Metrics & More | Article Recommendations | Supporting Information

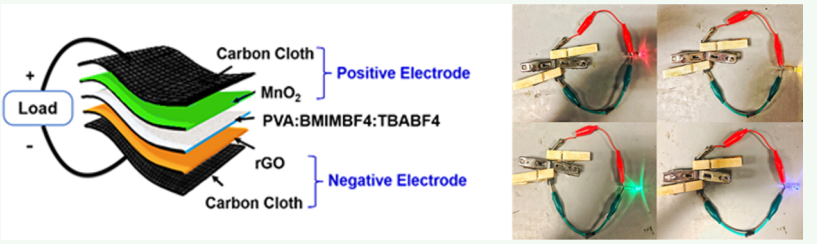

ABSTRACT: In the past years, all-solid-state supercapacitors, as energy storage devices, have drawn greatest attention in both academic and industrial sectors because of their potential applications, in particular in the wearable and portable electronics. However, poor energy densities of all-solid-state supercapacitors restrict their practical applications. In this study, we first report novel ionic liquid gels composed of poly(vinyl alcohol) (PVA), 1-butyl-3-methylimidazolium tetrafluoroborate (BMIMBF4), and tetrabutylammonium tetrafluoroborate (TBABF4) (PVA:BMIMBF4:TBABF4) as the solid-state electrolytes. It is found that the PVA:BMIMBF4:TBABF4 solid-state electrolytes exhibit dramatically enhanced ionic conductivity. Afterward, we report all-solid-state asymmetric supercapacitors (ASCs) by using MnO_2 coated on a carbon cloth (CC) as the positive electrode, reduced graphene oxide coated on a CC as the negative electrode, and novel PVA:BMIMBF4:TBABF4 as the solid-state electrolyte. All-solid-state ASCs exhibit an operational window of 3 V, an energy density of 61.2 W h/kg at the power density of 1049 W/kg, and more than 80% capacitance retention after 3000 charge/discharge cycles. All these results demonstrate that we provide a facile way to develop high-energy-density all-solid-state ASCs with good cycling stability.

KEYWORDS: *all-solid-state asymmetric supercapacitors, energy density, ionic liquid gels, solid-state electrolytes, flexibility*

INTRODUCTION

Supercapacitors, one of the energy storage devices, have drawn great attention in both academic and industrial sectors because of their high power density and cost-effective manufacturing.[1−3] In supercapacitors, charge carriers are stored in the interfaces between the electrodes and electrolytes,[4,5] which result in high power densities. However, poor energy densities restrict their practical applications, in particular in the wearable and smart electronics.[6−9]

Many approaches have been attempted to enhance the energy densities of supercapacitors.[1,10,11] To enlarge operational voltage (V) was demonstrated to be a simple way to enhance the energy density because the energy density is proportional to the square of V.[4,5] Toward this end, ionic liquids were used as electrolytes because supercapacitors incorporated with ionic liquid electrolytes could generate a large operational window (3−5 V).[12−15] Moreover, ionic liquids possess a low melting point, a low vapor pressure, and noninflammability,[15] which enable supercapacitors to be operated in a broad working temperature range, extending its applications.[16−19] However, poor ionic conductivities of ionic liquid electrolytes originating from large ionic sizes and high viscosities restricted supercapacitors to have high power densities.[16,20]

To boost the ionic conductivities of ionic liquid electrolytes, both polar and redox additives were incorporated with ionic liquids as electrolytes.[18,21,22] Yang et al.[18] observed an ∼25 mS/cm ionic conductivity from graphene oxide (GO) mixed with poly(vinylidene fluoride-hexafluoro propylene) [P(VDF-HFP)]-1-ethyl-3-methylimidazolium tetrafluoroborate (EMIMBF4) ionic gels and further found out that all-solid-state supercapacitors incorporated with GO-(P(VDF-HFP)-EMIMBF4 gel electrolytes exhibited a stable working potential window from 0 to 3.5 V, a specific capacitance of 190 F/g, and an energy density of 76 W h/kg at the current density of 1 A/g. However, the abovementioned fluoric copolymers possessed poor flexibility and a high cost.[18,23,24] Thus, polymer matrixes

Received: September 1, 2020
Accepted: November 11, 2020

with high flexibility as the solid-state electrolytes need to be developed for approaching high-energy-density supercapacitors.[18,19]

In this study, we first report novel ionic liquid gels composed of poly(vinyl alcohol) (PVA), 1-butyl-3-methylimidazolium tetrafluoroborate (BMIMBF4), and tetrabutylammonium (TBA) tetrafluoroborate (TBABF4) (PVA:BMIMBF4:TBABF4) as the solid-state electrolytes. It is found that the PVA:BMIMBF4:TBABF4 solid-state electrolytes exhibit an ionic conductivity of 21.7 mS/cm. We further assemble all-solid-state asymmetric supercapacitors (ASCs) by using MnO_2 coated on a carbon cloth (CC) (MnO_2@CC) as the positive electrode, reduced GO (rGO) coated on a CC (rGO@CC) as the negative electrode, and the PVA:BMIMBF4:TBABF4 ionic liquid gels as the solid-state electrolytes. ASCs exhibit an operational window of 3 V, an energy density of 61.2 W h/kg at the power density of 1049 W/kg, and more than 80% capacitance retention after 3000 charge/discharge cycles.

RESULTS AND DISCUSSION

Figure 1 shows the scanning electron microscopy (SEM) images of both PVA:BMIMBF4 and the PVA:BMIMBF4:TBABF4 gel electrolytes. In the solid-state electrolytes, PVA was used as a separator and polymer matrix, while BMIMBF4 and TBABF4 were mixed with PVA, serving as electrolytic salts. Similar to the SEM image of pure PVA gels (Supporting Information, SI 1), PVA:BMIMBF4 gel electrolytes possess a quite smooth surface, which indicates that a bulk compact structure is formed. Such a compact structure is ascribed to the good solubility of BMIMBF4 and PVA in dimethyl sulfoxide (DMSO) solutions. However, such a compact structure could slow down ionic transport from electrolytes to the electrodes. To circumvent this problem, TBABF4 is mixed with PVA:BMIMBF4 gels to form PVA:BMIMBF4:TBABF4 gel electrolytes because TBABF4 possesses different solubility in DMSO compared to BMIMBF4 in DMSO. Thus, the PVA:BMIMBF4:TBABF4 gel electrolytes possess tuned film morphologies.

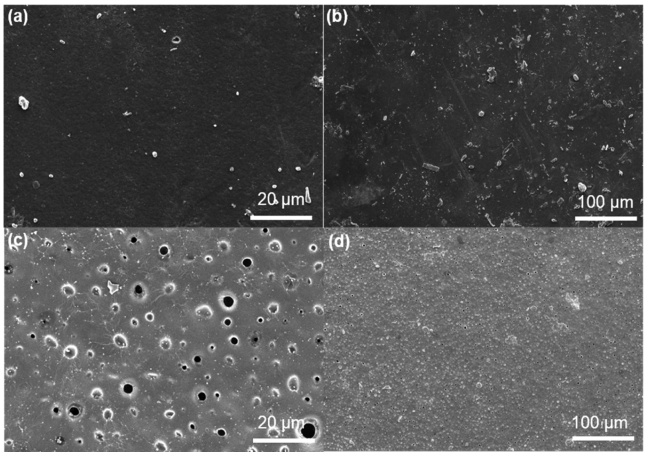

Figure 1. (a) High- and (b) low-magnification SEM images of the PVA:BMIMBF4 gel electrolytes and (c) high- and (d) low-magnification SEM images of PVA:BMIMBF4:TBABF4 gel electrolytes (a BMIMBF4/TBABF4 molar ratio of 4:1).

Figure 1c,d shows both high- and low-magnification SEM images of the PVA:BMIMBF4:TBABF4 gel electrolytes (where the mole ratio of BMIMBF4/TBABF4 is 4:1). The PVA:BMIMBF4:TBABF4 gel electrolytes possess a porous structure compared to the PVA:BMIMBF4 gel electrolytes. Such a porous structure is probably ascribed to the different solubility of TBABF4 in DMSO compared to that of BMIMBF4 in DMSO.[25] Most importantly, such a porous structure could provide channels for counterions to be efficiently transported from electrolytes to the electrode, resulting in boosted ionic conductivity.[26] However, as shown in Figure S1, a high concentration of TBABF4 in the PVA:BMIMBF4:TBABF4 gel electrolytes would induce phase separation and generate TBABF4 precipitation, resulting in decreased stability and ionic conductivity.

Figure 2a shows the cycling voltammetry (CV) curves of supercapacitors with a device configuration of CC//PVA:BMIMBF4:TBABF4//CC. Supercapacitors incorporated with the PVA:BMIMBF4:TBABF4 gel electrolytes maintain unchanged shapes of the CV curves under the scan rates from 10 to 75 mV/s, indicating that the PVA:BMIMBF4:TBABF4 gel electrolytes have good electrochemical stability. As indicated in Figure 2b, the area of the CV curve of supercapacitors incorporated with the PVA:BMIMBF4:TBABF4 gel electrolytes is larger than that incorporated with the PVA:BMIMBF4 gel electrolytes under the same scan rate. Such an enlarged area indicates that more counterions are efficiently transported. Furthermore, the areas of the CV curves of supercapacitors incorporated with the PVA:BMIMBF4:TBABF4 gel electrolytes are dramatically increased along with the increased scan rates, whereas the areas of the CV curves of supercapacitors incorporated with the PVA:BMIMBF4 gel electrolytes exhibit a negligible change along with the increased scan rates. These results demonstrate that the PVA:BMIMBF4:TBABF4 gel electrolytes possess efficient electrochemical double layers at the high scan rates as compared to the PVA:BMIMBF4 gel electrolytes (S1).[27]

Figure 2c,b displays the galvanostatic charge/discharge (GCD) curves of supercapacitors incorporated with either PVA:BMIMBF4 or PVA:BMIMBF4:TBABF4 gel electrolytes. It is found that the specific capacitances are increased to 17.5 mF/cm^2 for supercapacitors incorporated with PVA:BMIMBF4:TBABF4 gel electrolytes from 9.2 mF/cm^2 for supercapacitors incorporated with PVA:BMIMBF4 gel electrolytes. However, an operational voltage observed from supercapacitors incorporated with the PVA:BMIMBF4:TBABF4 gel electrolytes is 3 V, which is smaller than that (4 V) from the supercapacitor incorporated with the PVA:BMIMBF4 gel electrolytes (Figure 2b). Such a reduced operational voltage has probably originated from quaternary ammonium (TBA), which typically exhibited a smaller operational window.[28]

Figure 3a shows the Nyquist plots of supercapacitors with a device configuration of CC//gel electrolytes//CC, where the gel electrolyte is either PVA:BMIMBF4:TBABF4 or PVA:BMIMBF4. A series resistance (R_s) of ~100 Ω is observed from supercapacitors incorporated with the PVA:BMIMBF4 gel electrolytes, whereas an R_s of ~9.2 Ω is observed from supercapacitors incorporated with the PVA:BMIMBF4:TBABF4 gel electrolytes. Thus, the calculated ionic conductivity (the equation in the Supporting Information, SI 1) of the PVA:BMIMBF4:TBABF4 gel electrolytes is ~21.7 mS/cm, which is much higher than that (~1.9 mS/cm) for the PVA:BMIMBF4 gel electrolytes. Such a boosted ionic conductivity indicates that the PVA:BMIMBF4:TBABF4 gel electrolytes could enhance the electrochemical performance of supercapacitors.[29]

https://dx.doi.org/10.1021/acsaelm.0c00759
ACS Appl. Electron. Mater. XXXX, XXX, XXX−XXX

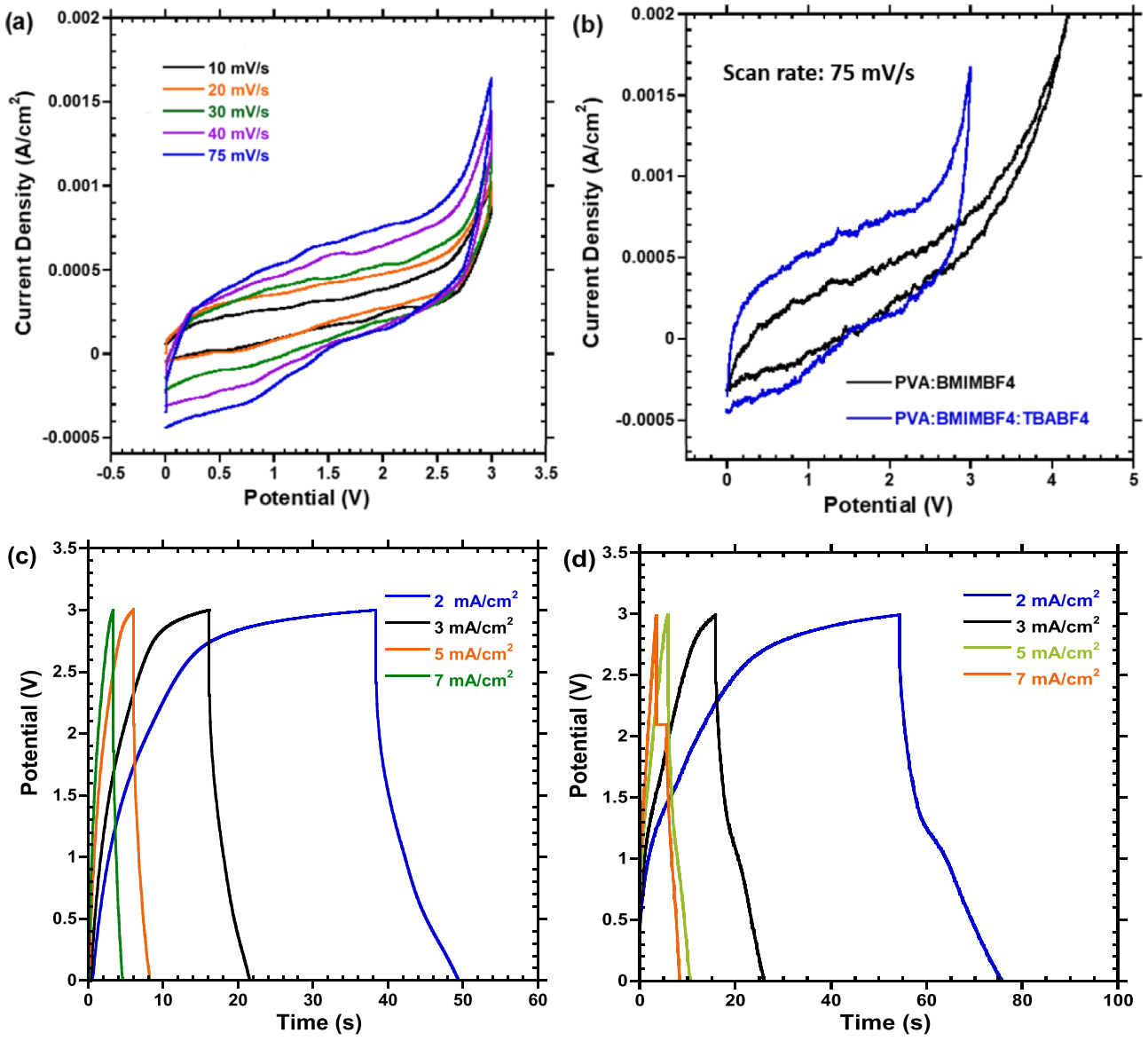

Figure 2. (a) CV curves of PVA:BMIMBF4:TBABF4 gel electrolytes, (b) Nyquist plots of PVA:BMIMBF4:TBABF4 and PVA:BMIMBF4 gel electrolytes, and GCD curves of supercapacitors incorporated with (c) PVA:BMIMBF4 and (d) PVA:BMIMBF4:TBABF4 gel electrolytes.

Figure 3b shows the Nyquist plots of supercapacitors with a device configuration of CC//PVA:BMIMBF4:TBABF4//CC tested at different temperatures. It is found that the R_s values are decreased to 4.3 Ω at 90 °C from 9.2 Ω at room temperature. These results indicate that such supercapacitors are able to work in a large temperature range,[29] which is inaccessible in aqueous systems because of the evaporation of water.

To further enhance the energy density, supercapacitors with an asymmetric device configuration are constructed. Studies indicated that transition-metal oxides were good positive electrode materials because of their excellent pseudocapacitive properties. Manganese oxides (MnO_2) as pseudocapacitive electrode materials have attracted much attention because of their high theoretical specific capacitance, natural abundance, and low toxicity. Thus, MnO_2 is selected as the positive electrode material. On the other hand, rGO, a typical low-dimensional carbon material, has been widely reported as the negative electrode material, which is ascribed to its large surface area, high electrical conductivity, and adjustable pore size. Thus, rGO is used as the negative electrode material. In order to enhance flexibility of supercapacitors, both MnO_2 and rGO are coated on the CC because a flexible CC could serve as a current collector and provide excellent flexibility to the supercapacitors.

The powder X-ray diffraction (XRD) characterization of the MnO_2@CC positive electrode and the transmission electron microscopy (TEM) characterization of the rGO@CC negative electrode are shown in the Supporting Information, SI 2. It is found that the diffraction peaks of the MnO_2@CC electrode are consistent with the reference peaks (JCPDS card no. 42-1169). Moreover, rGO shows an ultrathin nanosheet-like structure, which provides a large surface area for the rGO@CC electrode.

Figure 4a,b shows the CV and GCD curves of the MnO_2@CC positive electrode in BMIMBF4/TBABF4 (4:1 mole ratio) in acetonitrile (ACN) solution. The MnO_2@CC electrode shows a stable operational window from 0 to 1.5 V. No significant change is observed at the scan rates from 10 to 100 mV/s. These results indicate that the MnO_2@CC positive

https://dx.doi.org/10.1021/acsaelm.0c00759
ACS Appl. Electron. Mater. XXXX, XXX, XXX−XXX

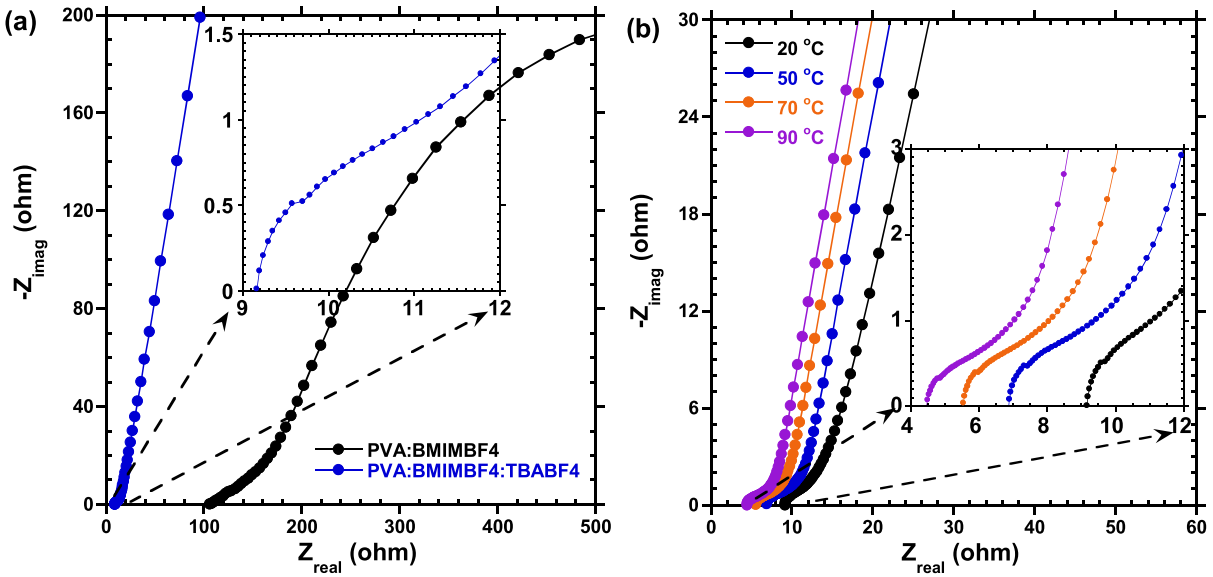

Figure 3. (a) Nyquist plots of supercapacitors incorporated with either the PVA:BMIMBF4:TBABF4 or PVA:BMIMBF4 gel electrolytes and (b) Nyquist plots of supercapacitors incorporated with the Pin VA:BMIMBF4:TBABF4 gel electrolytes at different working temperatures.

electrode can provide a rapid and reversible pseudocapacitance. Moreover, the largest specific capacitance is calculated to be 118.0 F/g at the current density of 0.5 A/g based on the GCD curves (Figure 4b) (Supporting Information, SI 2).

Figure 4c,d shows the CV and GCD curves of the rGO@CC negative electrode in BMIMBF4/TBABF4 (4:1 mole ratio) in ACN solution. The rGO@CC negative electrode exhibits an operational window from −1.7 to 0 V. No significant change is observed at the scan rates from 10 to 100 mV/s. These results demonstrate that the rGO@CC negative electrode is stable at the high current density. Moreover, the highest specific capacitance is calculated to be 95.4 F/g at the current density of 0.5 A/g (Supporting Information, SI 2) based on the GCD curves (Figure 4d).

Figure 4e shows the cycling stability of both the MnO_2@CC and rGO@CC electrodes. The increased capacitance in cycles from 300 to 500 from both the MnO_2@CC and rGO@CC electrodes is ascribed to the diffusion process of counterions from electrolytes to the electrodes. No significant degradation is observed from the rGO@CC electrode after 4000 charge/discharge cycles at the current density of 3 A/g. The MnO_2@CC electrode maintains 80% capacitance retention after 4000 charge/discharge cycles at the current density of 3 A/g. All these results reveal that both the MnO_2@CC and rGO@CC electrodes have good long-term cycling stabilities.

Figure 5a schematically displays the ASC device configuration, MnO_2@CC//PVA:BMIMBF4:TBABF4//rGO@CC, where MnO_2@CC and rGO@CC work as the positive electrode and the negative electrode, respectively, and the PVA:BMIMBF4:TBABF4 gels acts as the solid-state electrolytes. The CV curves of ASCs are presented in Figure 5b. ASCs exhibit a wide operational window from 0 to 3.0 V. No significant change is observed at the scan rates from 10 to 100 mV/s. These results indicate that ASCs have good electrochemical stability.

The GCD curves of ASCs at the current densities from 0.5 to 10 A/g are shown in Figure 5c. The ASCs show the highest specific capacitance of 49 F/g, an energy density of 61.2 W h/kg, and a power density of 1049 W/kg at the current density of 0.5 A/g (Supporting Information, SI 3). Figure 5d displays the Ragone plot of MnO_2@CC//PVA:BMIMBF4:TBABF4//rGO@CC ASCs. Compared to the recent reported works, such as supercapacitors incorporated with nanocellulose-enhanced active carbon, 1-butyl-1-methylpyrrolidinium bis(fluorosulfonyl)imide, graphene nanocomposites, and salt-templated carbon materials,[2,30−32] the MnO_2@CC//PVA:BMIMBF4:TBABF4//rGO@CC ASCs show both a high energy density and high power density. All these results demonstrate that the MnO_2@CC//PVA:BMIMBF4:TBABF4//rGO@CC ASCs have promising potential in high-performance wearable and portable devices.

Figure 5e shows the cycling stability of ASCs. The increased capacitance in the first 800 cycles is attributed to the diffusion of counterions from the PVA:BMIMBF4:TBABF4 gel electrolytes into the electrodes. The ASCs maintain greater than 80% capacitance retention after 3000 charge/discharge cycles at the current density of 3 A/g. These results demonstrate that ASCs exhibit good cycling stability.

The flexibility of ASCs is further investigated. Figure 6a displays the capacitance retention of ASCs under different bending angles. It is found that ASCs do not show any fracture and irreversible deformation under different bending angles from 30 to 120° (Supporting Information, SI 4). No significant changes are observed from ASCs bent under different bending angles (the inset of Figure 6a). Moreover, the capacitance retention calculated by the CV areas (Figure 6a) show negligible change under different bending angles and bending cycles (Supporting Information, SI 4). All these results indicate that ASCs possess good flexibility and mechanical stability.

The application of ASCs is further explored. As indicated in Figure 6b, light-emitting diodes (LEDs) can be lighted by two series-connected ASCs. Two series-connected ASCs are able to power not only the red and orange LEDs (turn-on voltage: 1.8−2.2 V) but also the green LED (turn-on voltage: 3.0−3.2 V) and blue LED (turn-on voltage: 2.5−3.7 V). These results demonstrate that ASCs possess great potential applications.

CONCLUSIONS

In this study, we reported all-solid-state ASCs by using MnO_2@CC as the positive electrode, rGO@CC as the

https://dx.doi.org/10.1021/acsaelm.0c00759
ACS Appl. Electron. Mater. XXXX, XXX, XXX−XXX

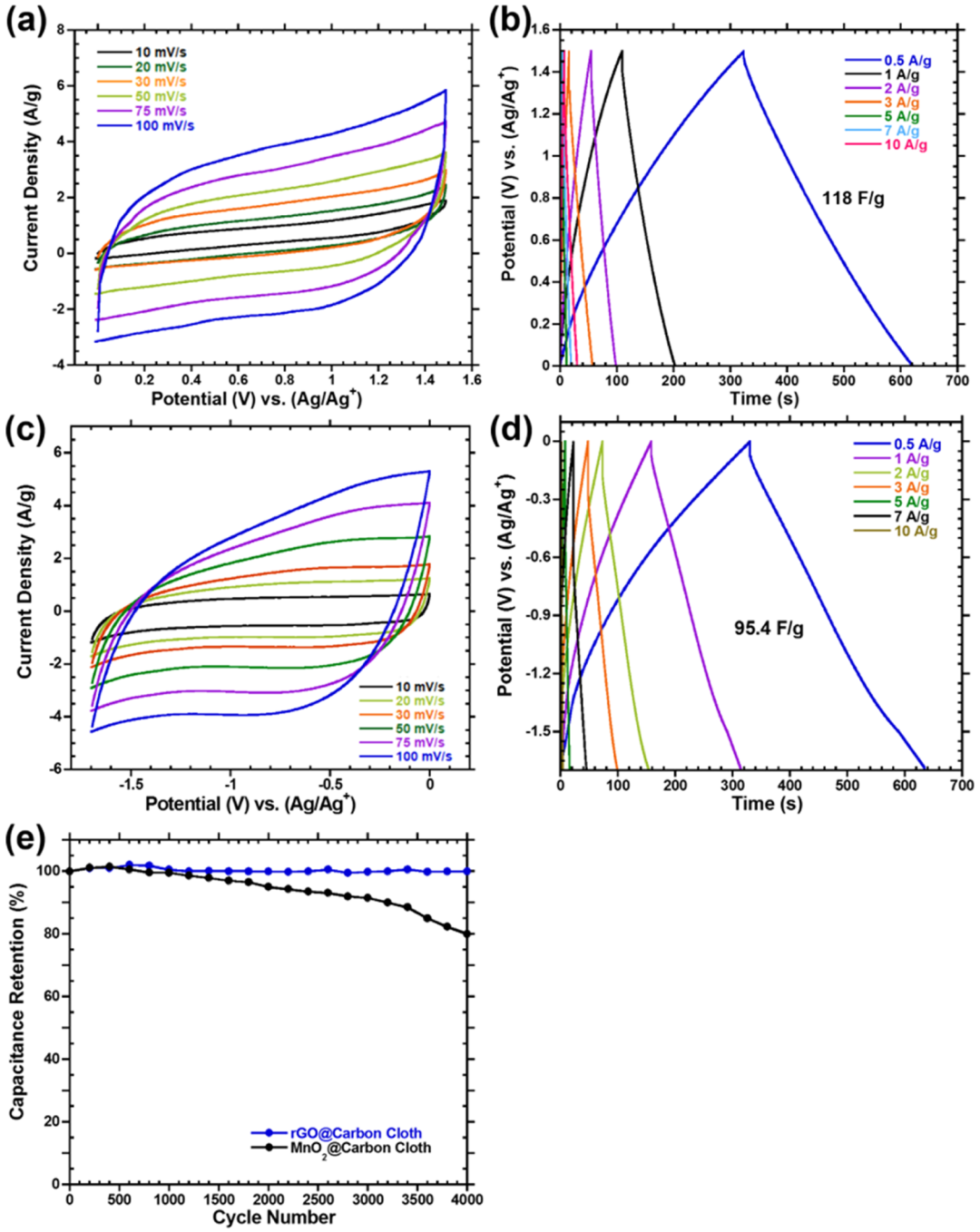

Figure 4. (a) CV curves and (b) GCD curves of the MnO_2@CC electrode, (c) CV curves and (d) GCD curves of the rGO@CC electrode, and (e) cycling stabilities of the MnO_2@CC and the rGO@CC electrodes.

negative electrode, and the PVA:BMIMBF4:TBABF4 gels as solid-state electrolytes. It was found that the PVA:BMIMBF4:TBABF4 gel electrolytes exhibited an enhanced ionic conductivity of 21.7 mS/cm compared to that (1.9 mS/cm) of the PVA:BMIMBF4 gel electrolytes. ASCs with a device configuration of MnO_2@CC//PVA:BMIMBF4:TBABF4//rGO@CC exhibited an operational window of 3.0 V, an energy density of 61.2 W h/kg at the power density of 1049 W/kg, and more than 80% capacitance retention after 3000 charge/discharge cycles. Moreover, ASCs can be used to light different LEDs with different turn-on voltages. All these results demonstrated that ASCs we developed have great potential applications in the high-performance wearable and portable devices.

EXPERIMENTAL SECTION

Materials. PVA (M_w 89,000−98,000, 99+% hydrolyzed), BMIMBF4, TBABF4, potassium permanganate ($KMnO_4$), graphite (powder, <20 μm, synthetic), manganese acetate [$Mn(CH_3COO)_2$], sodium sulfate (Na_2SO_4), and sodium dodecyl sulfonate were purchased from Sigma-Aldrich. The CC (0.5 mm thickness) was purchased from Fuel Cells Earth. ACN and DMSO were purchased from Fisher Chemical Co., Ltd. Phosphorus(V) oxide (P_2O_5) and potassium peroxydisulfate ($K_2S_2O_8$) were purchased from Alfa Aesar. All materials are used as received without further purification.

https://dx.doi.org/10.1021/acsaelm.0c00759
ACS Appl. Electron. Mater. XXXX, XXX, XXX−XXX

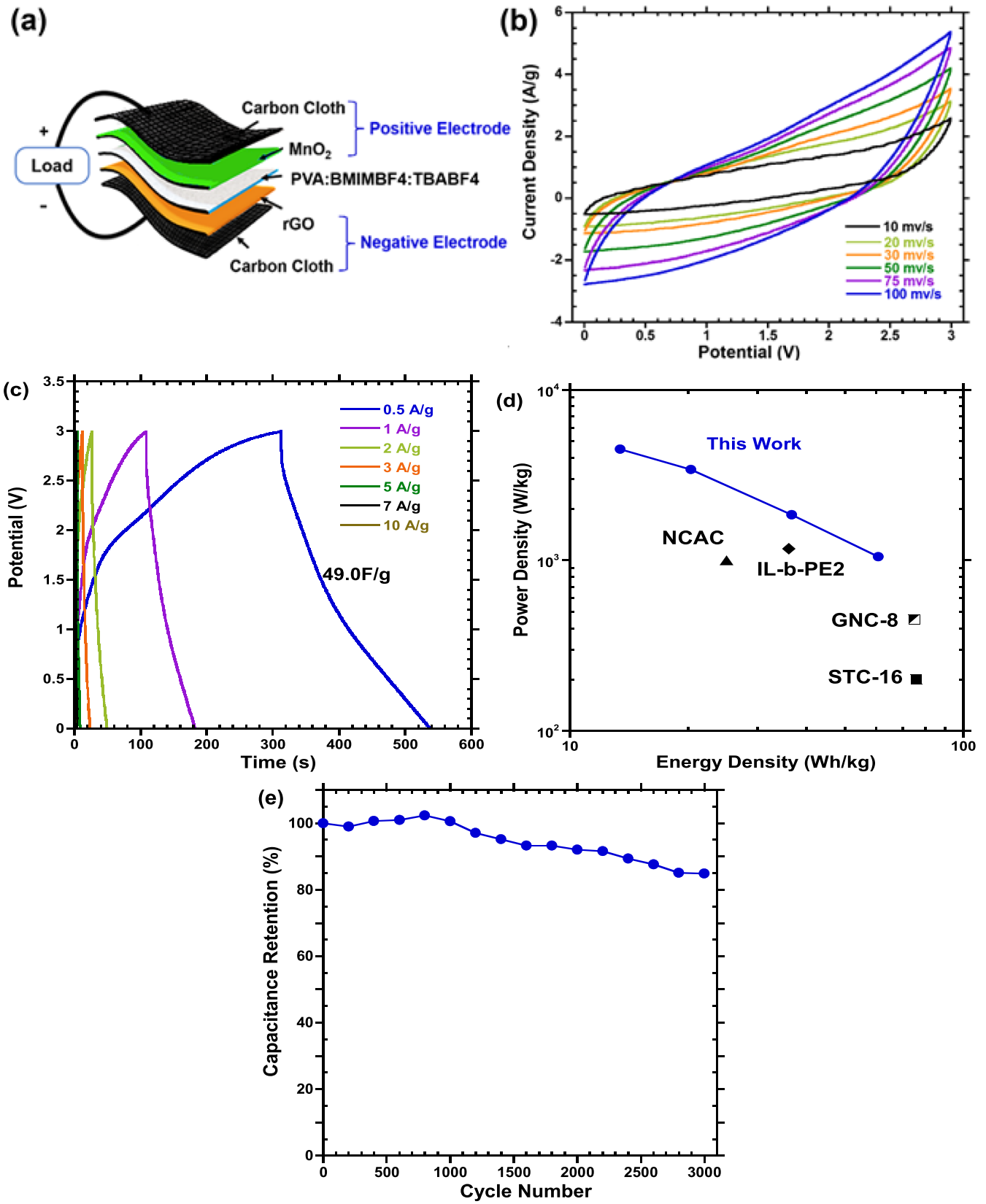

Figure 5. (a) Schematic illustration of the ASC device configuration, (b) CV curves, (c) GCD curves, (d) Ragone plot, and (e) cycling stability of MnO_2@CC//PVA:BMIMBF4:TBABF4//rGO@CC ASCs.

Synthesis of rGO. GO was synthesized following improved Hummers' method.[33] First, 3.0 g of graphite powder was mixed with 12 mL of 98% H_2SO_4. After that, 2.5 g of $K_2S_2O_8$ and 2.5 g of P_2O_5 powders were added into the above mixture solution, and the mixture solution was heated to 80 °C under stirring for 6 h. Afterward, the above solution was cooled down to room temperature naturally.

https://dx.doi.org/10.1021/acsaelm.0c00759
ACS Appl. Electron. Mater. XXXX, XXX, XXX−XXX

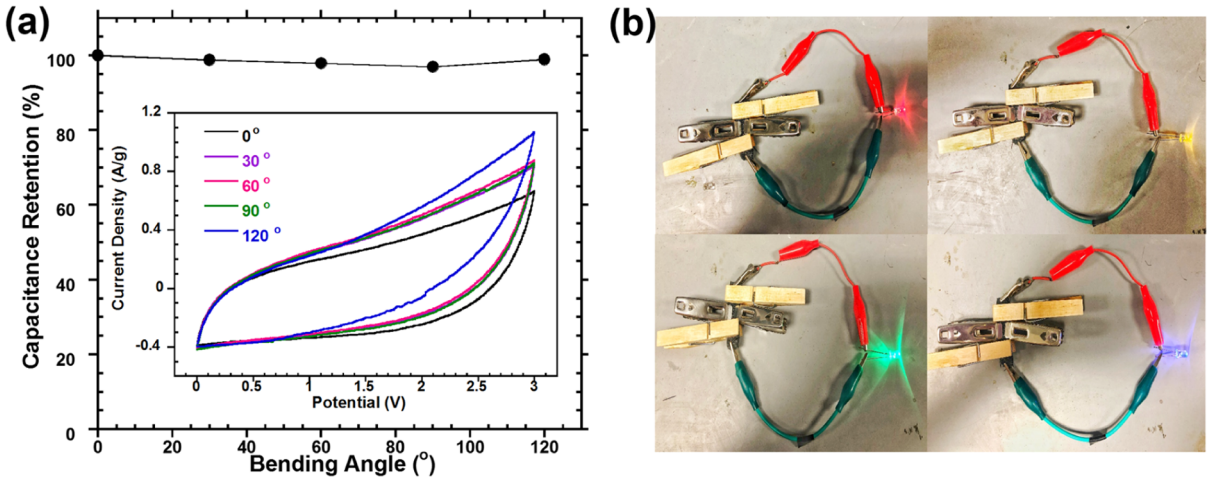

Figure 6. (a) Capacitance retention of ASCs under different bending angles; the inset of (a) shows the CV curves of ASCs under different bending angles. (b) Different LEDs lighted by two series-connected ASCs.

Under continuous stirring, 120 mL of cold H_2SO_4 solution was poured into the above mixture solution, followed by addition of 15 g of $KMnO_4$. This mixture solution was kept at a temperature less than 35 °C for 6 h. After that, 700 mL of deionized (DI) water was added into the above solution. 20 mL of H_2O_2 (30%) was added into the above solution to form a clear and yellowish solution. The above yellowish solution was further centrifuged and washed with 1 M HCl and then DI water several times. The product is GO solution. Afterward, 20 μL of hydrazine hydrates was added into 10 mL of the GO solution (~2 mg/mL). The mixture solution was heated in an autoclave at 60 °C for 6 h. Finally, rGO was dried in an oven at 60 °C for 12 h.

Synthesis of PVA:TBABF4:BMIMBF4 Gels. The PVA:TBABF4:BMIMBF4 gels were synthesized by a solution-cast method.[26] First, PVA solution was prepared by dissolving 1 g of PVA powder in 10 mL of DMSO under stirring. After 1 h stirring, 2.26 g of BMIMBF4 was added into the above solution. The mixture solution was stirred for 2 h at 60 °C. Then, TBABF4 powder (0 or 0.822 or 1.645 g) was dissolved in 1 mL of DMSO to make TBABF4 DMSO solution. The TBABF4 DMSO solution was dropped into the PVA:BMIMBF4 solution under vigorous stirring at 60 °C for 4 h to make homogeneous solutions (the molar ratios of BMIM/TBA are 1:0, 2:1, and 4:1). Finally, the above solution was put into a Petri dish and then dried in a vacuum oven at 80 °C for 8 h to produce transparent gels.

Preparation of the Electrodes. MnO_2 was electrochemically deposited on the top of the pretreated CC (1 cm × 1 cm) to form MnO_2@CC.[34] rGO was blended with carbon black and polyvinylidene difluoride in a weight ratio of 8:1:1 in 1-methyl-2-pyrrolidone. Then, the slurry containing rGO, carbon black, and polyvinylidene difluoride was coated on the pretreated CC (1 cm × 1 cm) and dried at 60 °C for 12 h.[2,35] Both the MnO_2@CC and rGO@CC electrodes were loaded around 3 mg of active materials with a total thickness of 0.6−0.7 mm.

Fabrication of ASCs. The MnO_2@CC//PVA:BMIMBF4:TBABF4//rGO@CC ASCs were fabricated by assembling MnO_2@CC as the positive electrode, rGO@CC as the negative electrode, and the PVA:BMIMBF4:TBABF4 gels as the solid-state electrolytes with a sandwich-type device configuration. The mass loaded on the two electrodes was calculated by eq S4 listed in the Supporting Information, SI 3. The total mass loaded on the two electrodes is around 3 mg. Finally, ASCs were packaged by the polyethylene terephthalate (PET) film.

Characterization of ASCs. SEM images of samples were obtained using a JEOL-7401. XRD was performed using a Rigaku SmartLab X-ray diffractometer. TEM was performed using a transmission electron microscope with type Tecnai G2 F20. The CV, GCD, and electrochemical impedance spectroscopy (EIS) measurements were performed using Gamry reference 3000 electrochemical workstations (Gamry Instruments, U.S.A). The single electrode was measured in a three-electrode configuration using the platinum wire and the Ag/Ag^+ electrode as the counter electrode and reference electrode, respectively. EIS was performed at the frequency ranging from 10 mHz to 100 kHz and an impedance amplitude of ±5 mV under open-circuit potential conditions. The cyclic stability was measured using a LAND CT2001A (Landt Instruments, Wuhan, China).

■ ASSOCIATED CONTENT

Supporting Information

The Supporting Information is available free of charge at https://pubs.acs.org/doi/10.1021/acsaelm.0c00759.

PVA:TBABF4:BMIMBF4 gel electrolytes, MnO_2@CC and rGO@CC electrodes, MnO_2@CC//PVA:BMIMBF4:TBABF4//rGO@CC ASCs, and flexibility of ASCs (PDF)

■ AUTHOR INFORMATION

Corresponding Author

Xiong Gong − *School of Polymer Science and Polymer Engineering, College of Engineering and Polymer Science, The University of Akron, Akron, Ohio 44325, United States;* orcid.org/0000-0001-6525-3824; Email: xgong@uakron.edu; Fax: (330) 9723406

Authors

Yongrui Yang − *School of Polymer Science and Polymer Engineering, College of Engineering and Polymer Science, The University of Akron, Akron, Ohio 44325, United States*

Tao Zhu − *School of Polymer Science and Polymer Engineering, College of Engineering and Polymer Science, The University of Akron, Akron, Ohio 44325, United States*

Cheng Chi − *School of Polymer Science and Polymer Engineering, College of Engineering and Polymer Science, The University of Akron, Akron, Ohio 44325, United States*

Lei Liu − *School of Polymer Science and Polymer Engineering, College of Engineering and Polymer Science, The University of Akron, Akron, Ohio 44325, United States*

Jie Zheng − *Department of Chemical and Biomolecular Engineering, College of Engineering and Polymer Science, The University of Akron, Akron, Ohio 44325, United States;* orcid.org/0000-0003-1547-3612

https://dx.doi.org/10.1021/acsaelm.0c00759
ACS Appl. Electron. Mater. XXXX, XXX, XXX−XXX

Complete contact information is available at:
https://pubs.acs.org/10.1021/acsaelm.0c00759

Author Contributions

[§]Y.Y., T.Z., and C.C. contributed to this work equally.

Notes

The authors declare no competing financial interest.

■ ACKNOWLEDGMENTS

The authors thank the National Science Foundation (EECs 1903303) and the Air Force Office of Scientific Research (AFOSR) (through the Organic Materials Chemistry Program, grant number: FA9550-15-1-0292, Program Manager, Dr. Kenneth Caster) for financial support.

■ REFERENCES

(1) Mourad, E.; Coustan, L.; Lannelongue, P.; Zigah, D.; Mehdi, A.; Vioux, A.; Freunberger, S. A.; Favier, F.; Fontaine, O. Biredox ionic liquids with solid-like redox density in the liquid state for high-energy supercapacitors. *Nat. Mater.* **2017**, *16*, 446.
(2) Li, Z.; Liu, J.; Jiang, K.; Thundat, T. Carbonized nanocellulose sustainably boosts the performance of activated carbon in ionic liquid supercapacitors. *Nano Energy* **2016**, *25*, 161−169.
(3) Béguin, F.; Presser, V.; Balducci, A.; Frackowiak, E. Carbons and electrolytes for advanced supercapacitors. *Adv. Mater.* **2014**, *26*, 2219−2251.
(4) Wang, G.; Zhang, L.; Zhang, J. A review of electrode materials for electrochemical supercapacitors. *Chem. Soc. Rev.* **2012**, *41*, 797−828.
(5) Zhong, C.; Deng, Y.; Hu, W.; Qiao, J.; Zhang, L.; Zhang, J. A review of electrolyte materials and compositions for electrochemical supercapacitors. *Chem. Soc. Rev.* **2015**, *44*, 7484−7539.
(6) Song, Z.; Duan, H.; Miao, L.; Ruhlmann, L.; Lv, Y.; Xiong, W.; Zhu, D.; Li, L.; Gan, L.; Liu, M. Carbon hydrangeas with typical ionic liquid matched pores for advanced supercapacitors. *Carbon* **2020**, *168*, 499−507.
(7) Yan, J.; Miao, L.; Duan, H.; Zhu, D.; Lv, Y.; Xiong, W.; Li, L.; Gan, L.; Liu, M. Core-shell hierarchical porous carbon spheres with N/O doping for efficient energy storage. *Electrochim. Acta* **2020**, *358*, 136899.
(8) Zhou, Z.; Miao, L.; Duan, H.; Wang, Z.; Lv, Y.; Xiong, W.; Zhu, D.; Li, L.; Liu, M.; Gan, L. Highly active N, O-doped hierarchical porous carbons for high-energy supercapacitors. *Chin. Chem. Lett.* **2020**, *31*, 1226−1230.
(9) Jost, K.; Stenger, D.; Perez, C. R.; McDonough, J. K.; Lian, K.; Gogotsi, Y.; Dion, G. Knitted and screen printed carbon-fiber supercapacitors for applications in wearable electronics. *Energy Environ. Sci.* **2013**, *6*, 2698−2705.
(10) Merlet, C.; Péan, C.; Rotenberg, B.; Madden, P. A.; Daffos, B.; Taberna, P. L.; Simon, P.; Salanne, M. Highly confined ions store charge more efficiently in supercapacitors. *Nat. Commun.* **2013**, *4*, 2701.
(11) Augustyn, V.; Come, J.; Lowe, M. A.; Kim, J. W.; Taberna, P.-L.; Tolbert, S. H.; Abruña, H. D.; Simon, P.; Dunn, B. High-rate electrochemical energy storage through Li+ intercalation pseudocapacitance. *Nat. Mater.* **2013**, *12*, 518−522.
(12) Armand, M.; Endres, F.; MacFarlane, D. R.; Ohno, H.; Scrosati, B. Ionic-liquid materials for the electrochemical challenges of the future. *Nat. Mater.* **2009**, *8*, 621−629.
(13) Frackowiak, E.; Lota, G.; Pernak, J. Room-temperature phosphonium ionic liquids for supercapacitor application. *Appl. Phys. Lett.* **2005**, *86*, 164104.
(14) Shim, Y.; Kim, H. J. Nanoporous carbon supercapacitors in an ionic liquid: a computer simulation study. *ACS Nano* **2010**, *4*, 2345−2355.
(15) Van Aken, K. L.; Beidaghi, M.; Gogotsi, Y. Formulation of ionic-liquid electrolyte to expand the voltage window of supercapacitors. *Angew. Chem., Int. Ed.* **2015**, *54*, 4806−4809.
(16) Rennie, A. J. R.; Sanchez-Ramirez, N.; Torresi, R. M.; Hall, P. J. Ether-bond-containing ionic liquids as supercapacitor electrolytes. *J. Phys. Chem. Lett.* **2013**, *4*, 2970−2974.
(17) Torop, J.; Palmre, V.; Arulepp, M.; Sugino, T.; Asaka, K.; Aabloo, A. Flexible supercapacitor-like actuator with carbide-derived carbon electrodes. *Carbon* **2011**, *49*, 3113−3119.
(18) Yang, X.; Zhang, L.; Zhang, F.; Zhang, T.; Huang, Y.; Chen, Y. A high-performance all-solid-state supercapacitor with graphene-doped carbon material electrodes and a graphene oxide-doped ion gel electrolyte. *Carbon* **2014**, *72*, 381−386.
(19) Pandey, G. P.; Hashmi, S. A. Ionic liquid 1-ethyl-3-methylimidazolium tetracyanoborate-based gel polymer electrolyte for electrochemical capacitors. *J. Mater. Chem. A* **2013**, *1*, 3372−3378.
(20) Tamailarasan, P.; Ramaprabhu, S. Carbon nanotubes-graphene-solidlike ionic liquid layer-based hybrid electrode material for high performance supercapacitor. *J. Phys. Chem. C* **2012**, *116*, 14179−14187.
(21) Liu, K.; Wu, J. Boosting the performance of ionic-liquid-based supercapacitors with polar additives. *J. Phys. Chem. C* **2016**, *120*, 24041−24047.
(22) Senthilkumar, S. T.; Selvan, R. K.; Melo, J. S. Redox additive/active electrolytes: a novel approach to enhance the performance of supercapacitors. *J. Mater. Chem. A* **2013**, *1*, 12386−12394.
(23) Pan, Z.; Yang, J.; Zhang, Q.; Liu, M.; Hu, Y.; Kou, Z.; Liu, N.; Yang, X.; Ding, X.; Chen, H.; Li, J.; Zhang, K.; Qiu, Y.; Li, Q.; Wang, J.; Zhang, Y. All-solid-state fiber supercapacitors with ultrahigh volumetric energy density and outstanding flexibility. *Adv. Energy Mater.* **2019**, *9*, 1802753.
(24) Dubal, D. P.; Chodankar, N. R.; Kim, D.-H.; Gomez-Romero, P. Towards flexible solid-state supercapacitors for smart and wearable electronics. *Chem. Soc. Rev.* **2018**, *47*, 2065−2129.
(25) Snedden, P.; Cooper, A. I.; Scott, K.; Winterton, N. Cross-Linked Polymer-Ionic Liquid Composite Materials. *Macromolecules* **2003**, *36*, 4549−4556.
(26) Chen, Z.; Yang, Y.; Ma, Z.; Zhu, T.; Liu, L.; Zheng, J.; Gong, X. All-Solid-State Asymmetric Supercapacitors with Metal Selenides Electrodes and Ionic Conductive Composites Electrolytes. *Adv. Funct. Mater.* **2019**, *29*, 1904182.
(27) Nicholson, R. S. Theory and application of cyclic voltammetry for measurement of electrode reaction kinetics. *Anal. Chem.* **1965**, *37*, 1351.
(28) Deschamps, M.; Gilbert, E.; Azais, P.; Raymundo-Piñero, E.; Ammar, M. R.; Simon, P.; Massiot, D.; Béguin, F. Exploring electrolyte organization in supercapacitor electrodes with solid-state NMR. *Nat. Mater.* **2013**, *12*, 351−358.
(29) Lin, R.; Taberna, P.-L.; Fantini, S.; Presser, V.; Pérez, C. R.; Malbosc, F.; Rupesinghe, N. L.; Teo, K. B. K.; Gogotsi, Y.; Simon, P. Capacitive Energy Storage from −50 to 100 °C Using an Ionic Liquid Electrolyte. *J. Phys. Chem. Lett.* **2011**, *2*, 2396−2401.
(30) Feng, L.; Wang, K.; Zhang, X.; Sun, X.; Li, C.; Ge, X.; Ma, Y. Flexible solid-state supercapacitors with enhanced performance from hierarchically graphene nanocomposite electrodes and ionic liquid incorporated gel polymer electrolyte. *Adv. Funct. Mater.* **2018**, *28*, 1704463.
(31) Tiruye, G. A.; Muñoz-Torrero, D.; Palma, J.; Anderson, M.; Marcilla, R. Performance of solid state supercapacitors based on polymer electrolytes containing different ionic liquids. *J. Power Sources* **2016**, *326*, 560−568.
(32) Yan, R.; Antonietti, M.; Oschatz, M. Toward the experimental understanding of the energy storage mechanism and ion dynamics in ionic liquid based supercapacitors. *Adv. Energy Mater.* **2018**, *8*, 1800026.
(33) Hummers, W. S., Jr.; Offeman, R. E. Preparation of graphitic oxide. *J. Am. Chem. Soc.* **1958**, *80*, 1339.
(34) Chen, Z.; Zheng, L.; Zhu, T.; Ma, Z.; Yang, Y.; Wei, C.; Liu, L.; Gong, X. All-solid-state flexible asymmetric supercapacitors fabricated

by the binder-free hydrophilic carbon cloth@MnO_2 and Hydrophilic carbon cloth@polypyrrole electrodes. *Adv. Electron. Mater.* **2019**, *5*, 1800721.

(35) Yang, J.; Duan, X.; Guo, W.; Li, D.; Zhang, H.; Zheng, W. Electrochemical performances investigation of NiS/rGO composite as electrode material for supercapacitors. *Nano Energy* **2014**, *5*, 74−81.

https://dx.doi.org/10.1021/acsaelm.0c00759
ACS Appl. Electron. Mater. XXXX, XXX, XXX−XXX